

Mammogram Segmentation by Contour Searching and Mass Lesions Classification With Neural Network

D. Cascio, F. Fauci, R. Magro, G. Raso, R. Bellotti, F. De Carlo, S. Tangaro, G. De Nunzio, M. Quarta, G. Forni, A. Lauria, M. E. Fantacci, A. Retico, G. L. Masala, P. Oliva, S. Bagnasco, S. C. Cheran, and E. Lopez Torres

Abstract—The mammography is the most effective procedure for an early diagnosis of the breast cancer. In this paper, an algorithm for detecting masses in mammographic images will be presented. The database consists of 3762 digital images acquired in several hospitals belonging to the MAGIC-5 collaboration (Medical Applications on a Grid Infrastructure Connection). A reduction of the whole image's area under investigation is achieved through a segmentation process, by means of a ROI Hunter algorithm, without loss of meaningful information. In the following classification step, feature extraction plays a fundamental role: some features give geometrical information, other ones provide shape parameters. Once the features are computed for each ROI, they are used as inputs to a supervised neural network with momentum. The output neuron provides the probability that the ROI is pathological or not. Results are provided in terms of ROC and FROC curves: the area under the ROC curve was found to be $A_z = 0.862 \pm 0.007$, and we get a 2.8 FP/Image at a sensitivity of 82%. This software is included in the CAD station actually working in the hospitals belonging to the MAGIC-5 Collaboration.

Index Terms—Breast cancer, image processing, mammography, neural network.

I. INTRODUCTION

BREAST cancer is one of the most common kinds of cancer, as well as the leading cause of mortality among women. It first appears as an asymptomatic lesion of the breast, then it may spread over the whole organ.

A study made on 100 000 women between 1995–1998 in the European Union reports 39.4 deaths/yr, regardless of the

Manuscript received November 12, 2004; revised April 26, 2006.

D. Cascio, F. Fauci, R. Magro, and G. Raso are with the Dipartimento di Fisica e Tecnologie Relative, Università di Palermo, Palermo, Italy. They are also with INFN, Sezione di Catania, Catania, Italy.

R. Bellotti, F. De Carlo, and S. Tangaro are with the Dipartimento di Fisica, Università di Bari, Bari, Italy. They are also with INFN, Sezione di Bari, Bari, Italy.

G. De Nunzio is with the Dipartimento di Scienza dei Materiali, Università di Lecce, Lecce, Italy. He is also with INFN, Sezione di Lecce, Lecce, Italy.

M. Quarta is with the Dipartimento di Matematica, Università di Lecce, Lecce, Italy. He is also with INFN, Sezione di Lecce, Lecce, Italy.

G. Forni is with the Dipartimento di Scienze Fisiche, Università di Napoli, Napoli, Italy. He is also with INFN, Sezione di Napoli, Napoli, Italy.

A. Lauria is with the Dipartimento di Matematica e Fisica, Università di Sassari, Sassari, Italy. He is also with INFN, Sezione di Napoli, Napoli, Italy.

M. E. Fantacci and A. Retico are with the Dipartimento di Fisica, Università di Pisa, Pisa, Italy. They are also with INFN, Sezione di Pisa, Pisa, Italy.

G. L. Masala and P. Oliva are with the Dipartimento di Matematica e Fisica, Università di Sassari, Sassari, Italy. They are also with the INFN, Sezione di Cagliari, Cagliari, Italy.

S. Bagnasco is with INFN, Sezione di Torino, Torino, Italy.

S. C. Cheran is with INFN, Sezione di Torino, Torino, Italy. He is also with the Dipartimento di Informatica, Università di Torino, Torino, Italy.

E. L. Torres is with CEADEN, Havana, Cuba.

Color versions of Figs. 2–4 available online at <http://ieeexplore.ieee.org>.

Digital Object Identifier 10.1109/TNS.2006.878003

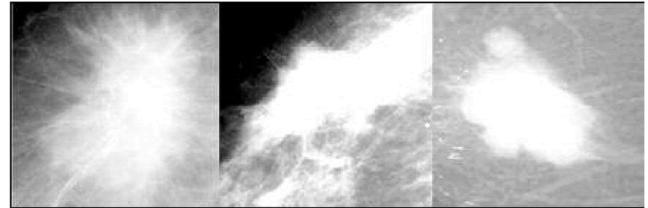


Fig. 1. Some examples of mass lesions selected from the database.

age, against 40.2 between 1985–1989, showing a change in rate equal to -2.1% . The favorable trend is due to therapeutic advancements, screenings, and earlier diagnosis [1].

Mammography is the most effective procedure for an early diagnosis of the anomalies which could mark a tumor, even if the detection of a tumor in a mammographic image is a difficult task [2], [3] due to the great number of nonpathological structures. Retrospective studies show that, in current breast cancer screenings, 10%–25% of the tumors are missed by the radiologists [4]. The causes of these false-negative screening examinations are not clear. The clinical significance of the early diagnosis and the difficulty of the diagnostic task have generated a tremendous interest in developing computer-aided detection (CAD) schemes for mammographic interpretations. The identification of masses [5]–[7] requires a dedicated strategy: shape and dimension of the masses are often irregular (Fig. 1), the borders are ill-defined, thus making difficult the discrimination from parenchyma's structures [8], [9]. In this paper, an algorithm for mass detection in mammography will be presented.

II. DATABASE

The mammograms used in this study belong to the MAGIC-5 database [10], [11], obtained by digitalization of the images collected in the hospitals of the collaboration. Images were acquired using different mammographic screen/film systems and settings (all with molybdenum anode) and within the framework of different applications, including both clinical routine carried out on symptomatic women, and screening programs addressed to asymptomatic women. Statistical distributions on patients age of the images present in the database are reported in Fig. 2.

Two views, mediolateral oblique and craniocaudal, were obtained with a standard analog mammography, and digitized with a scanner at a pixel resolution of $85 \mu\text{m} \times 85 \mu\text{m}$ [12]. Each image is thus 2657×2067 pixels and a grey value resolution of 12 bit. The total dataset consists of two-view and four-view mammograms, resulting in a total 3762 images, belonging to 1093 subjects. All images are characterized by a full description,

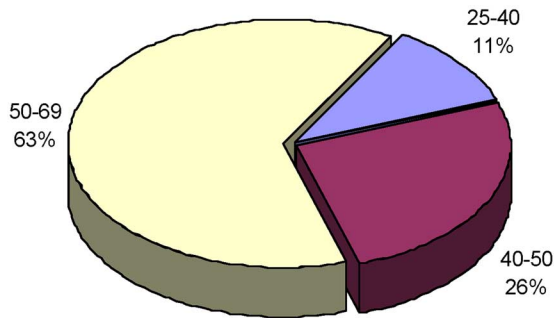


Fig. 2. Statistical distribution on age of the images in the database.

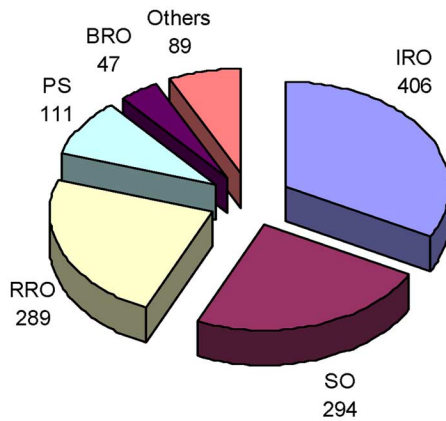


Fig. 3. Different kinds of masses present in the database. Legend: IRO = Irregular Roundish Opacity; SO = Spiculated Opacity; RRO = Regular Roundish Opacity; PS = Parenchymal Distorsion; BRO = Blurred Roundish Opacity; "others" include a combination of the aforementioned kinds.

e.g., radiologist diagnosis, tissue and lesion type. Images presenting only microcalcifications were excluded from our analysis. The mass dataset consists of 1153 pathological images, belonging to 608 patients, with at least one biopsy proven mass, and 2609 normal images without pathology, normal dataset, corresponding to patients with at least three years of follow-up. Each pathological image comes with a description of the lesion including radiological diagnosis, histological data and type of mass, as shown in Fig. 3. The total number of masses is 1236 from which 10% are of benign type. The location and size of a mass are defined by a radiologist-drawn circle in the digitized image: this action automatically creates a file containing the center coordinates (X_{Rad} ; Y_{rad}) and the radius (R_{Rad}) of the circle containing the mass; R_{Rad} ranges from 1.6 to 23.6 mm and has an average of 5.8 mm.

As far as the breast background is concerned, many Italian radiologists use the following standard tissue classification [13]:

- Fibro-adipose tissue: indicates a fat breast with little fibrous connective tissue;
- Glandular tissue: indicates the presence of prominent duct patterns;
- Dense tissue: indicates a dense breast parenchyma.

Fig. 4 reports the breast background composition of the database. Most of the images are glandular-like: the detection of pathological structures in this kind of images is a quite hard task, since the target is surrounded by a "noisy" environment.

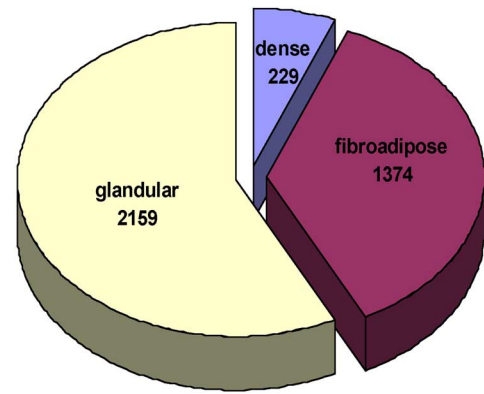


Fig. 4. Breast background composition of the database.

III. SEGMENTATION METHOD

An important step in CAD algorithms is the segmentation of the mammographic image. The goal of this step is to extract one or more regions of interest (ROIs) from the background. This is not a trivial task, due to the ill-defined borders, which make difficult their discrimination from the parenchyma's structures. The accuracy of this process will affect strongly the following classification step.

Usually, segmentation methods can be divided into two main categories: region-based and edge-based methods. In this work, we use an edge-based algorithm.

The contour search is carried out using a threshold operator which assigns the value I^+ to the pixel with the intensity greater than a fixed threshold, and I^- to the pixel with the intensity less than the threshold

$$\begin{aligned} \text{if } I_{x,y} \geq \text{threshold} &\Rightarrow I'_{x,y} = I^+ \\ \text{if } I_{x,y} < \text{threshold} &\Rightarrow I'_{x,y} = I^- \end{aligned}$$

where $I_{x,y}$ is the intensity for the pixel with coordinates (x, y).

One way to fix the threshold value is to draw an histogram of the pixel intensity on the whole image. Usually, this histogram has two peaks: the first one refers to the image background and the second one to the ROIs. The threshold may be chosen at the intensity corresponding to the crossover between the two peaks. This is a static selection criterion. In this paper we prefer to use a dynamical selection method as explained at point 3.

An iterative procedure (*ROI Hunter*), based on the search of relative intensity maximum inside a square window, has been implemented to select the ROIs. In the literature the mass lesions typically vary in size from 2–40 mm in diameters [14]; in our case these two limits correspond to the square windows limit: A_{min} (25×25), A_{max} (501×501), in pixel. All the ROIs with area less than A_{min} are removed.

The steps of the algorithm are as follows:

- starting from the right top corner of the mammogram, a raster scanning is performed to find the coordinates (x_o, y_o) of an intensity maximum I_m (the initial center of the candidate lesion). Its value is accepted if it is also a relative maximum in a box A_{min} (25×25 pixels);
- an iso-intensity contour, including the relative maximum intensity pixel, is drawn at a threshold value $I_{th} = I_m/2$; this contour defines a ROI with area A_R ;

$$\epsilon = 93\%; \text{ FP/image} = 7,8$$

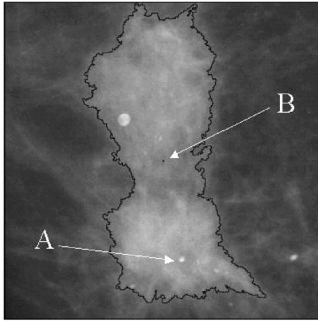


Fig. 5. A typical result of a ROI hunter processing; the starting point (A) and the luminosity mass center (B) are reported too.

- iii) the threshold I_{th} is dynamically changed by increasing/decreasing its value if the Area A_R of the corresponding ROI is greater/smaller than the limit area A_{max} (501×501 pixels), until the difference between two consecutive thresholds is equal to one. At each step, the threshold is changed by an amount which is one half of the previous one.
- iv) the ROI is removed and stored for a further analysis; the corresponding “hole” left in the mammogram is set to zero;
- v) go to step 1 to find next (x_o, y_o) coordinates of a relative intensity maximum.

To test and optimize the algorithm performance, we randomly divided the whole database in two equal sizes parts with similar characteristics; the first one was used to create two files: the training set and the validation set; both files were used to optimize the neural network; the second one was used to get the FROC curve of the CAD and to extract the test pattern. We have not distinguished between benign/malignant in our dataset analysis because we aimed to submit both cases and delay up to the histological examination the confirmation of the malignant pathology.

The rate detection value and the FP/image number, calculated by using all the database, are as follows: $\epsilon = 93\%$; $\text{FP/image} = 7.8$.

The mean area of the selected ROIs is approximately 16% of the whole mammogram.

In order to calculate the features that will be used in the classification system, it is reasonable to compute the luminosity mass center for each ROI. Fig. 5 reports a typical result obtained by using the ROI Hunter; the starting point (maximum intensity) and the luminosity mass center are marked with A and B, respectively. In the Fig. 6 we report the whole processing on a mammogram: the original image (left), the image without the ROIs (middle), and the extracted ROIs (right).

IV. FEATURE EXTRACTION

The ROI hunter provides the “regions of interest” without giving further information. To this purpose suitable features should be selected so that a decision making system can correctly classify possible pathological regions from healthy ones [15]–[17]. Feature extraction plays a fundamental role in

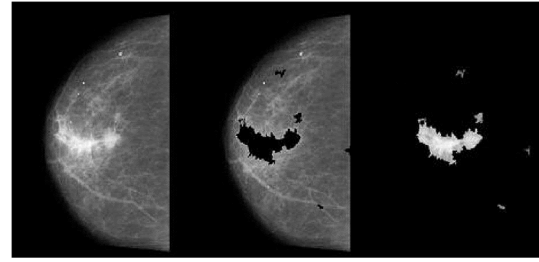


Fig. 6. The original image (left), the image without the ROI (middle) the extracted ROI (right).

TABLE I
LIST OF THE FEATURES USED

<i>Circularity</i>	<i>Inertial Momentum</i>
<i>Mean Radial Length</i>	<i>Entropy of contour gradient</i>
<i>Std of the Radial Length.</i>	<i>Anisotropy</i>
<i>Entropy of intensity distribution</i>	<i>Mean Intensity</i>
<i>Fractal index</i>	<i>Std of the Intensity</i>
<i>Eccentricity</i>	<i>Area</i>

many pattern recognition tasks. In this paper, 12 features are extracted from the segmented masses. The criteria for the feature selection are based on morphological differences between pathological and healthy regions; for example, the excessive lengthening (eccentricity) is often a symptom of the absence of pathology while the increase of the fractal index and the entropy of intensity in the lesion structures can mark a tumor. In Table I, the complete list of the features is reported.

Some features give geometrical information as eccentricity, area and average radial length; other ones provide shape parameters as fractal index, entropy, and inertial momentum. In the following, we will describe each of them.

A. Circularity

The circularity roughly describes the shape. It is defined as

$$C = P^2/A$$

where P and A are the perimeter and the area of the ROI, respectively.

B. Mean and Standard Deviation of the Radial Length

To get more information from the boundary two additional parameters are necessary:

- 1) the radial length measure R , defined as the mean of the euclidean distance R_k between the geometric center of the ROI, (X_0, Y_0) , and a point k on the boundary, normalized to the maximum radial length;
- 2) the standard deviation σ of the normalized radial length, computed over all the N boundary points of the ROI;

$$R = \frac{1}{N} \sum_{k=1}^N R_k \quad \sigma = \sqrt{\frac{1}{N} \sum_{k=1}^N (R_k - R)^2}$$

$$X_0 = \frac{1}{N} \sum_{i=1}^N x_i \quad \text{and} \quad Y_0 = \frac{1}{N} \sum_{i=1}^N y_i.$$

C. Entropy of the Intensity Distribution

The entropy measure E_I of a ROI, computed from the pixel intensity distribution, is given by

$$E_I = - \sum_{k=1}^{4096} p_k \log(p_k)$$

where p_k is the probability that the k th intensity value falls between I and $I + \Delta I$. This feature provides information about the flatness and roughness of the ROI.

D. Fractal Index

The fractal index is computed by means of the “box-counting” method. It consists in considering a squared grid (of side length L) on the image, and counting the number M of boxes which are superimposed to the ROI, for different box sizes L . The *Kolmogorof dimension* D (fractal index) of the ROI is given by

$$M \propto L^{-D}.$$

In case of ideal isotropic conditions, D corresponds to the *Hausdorff dimension*.

E. Eccentricity

The eccentricity characterizes the lengthening of a ROI. To this purpose a symmetric matrix \mathbf{A} is defined as follows:

$$\begin{aligned} A_{1,1} &= \sum_{i=1}^N (x_i - X_0)^2 \\ A_{2,2} &= \sum_{i=1}^N (y_i - Y_0)^2 \\ A_{1,2} &= A_{2,1} = \sum_{i=1}^N (x_i - X_0) \cdot (y_i - Y_0) \end{aligned}$$

where N is the contour pixels number, x_i and y_i are the coordinates of a generic pixel of the contour, X_0 and Y_0 are the coordinates of the geometric center of the ROI.

If λ_1 and λ_2 are the eigenvalues of the \mathbf{A} matrix, in the elliptical approximation of the ROI region, the semi-axis values will be

$$S_1 = \sqrt{\left| \frac{\lambda_1}{2} \right|} \quad S_2 = \sqrt{\left| \frac{\lambda_2}{2} \right|}.$$

Then the eccentricity is given by

$$\text{Eccentricity} = \frac{S_1}{S_2}$$

with $S_1 < S_2$. An Eccentricity close to 1 denotes a ROI like a circle, while values close to zero mean more stretched ROIs.

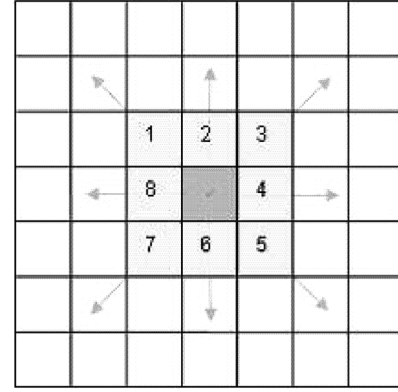


Fig. 7. A pixel of the contour is shown by the black square. The related gradient value will be oriented in the direction of the maximum change.

F. Inertial Momentum

The luminosity inertial momentum is defined as

$$\text{Inertial} = \sum_{k=1}^M I_k h_k^2$$

where h_k is the Euclidean distance of the k th pixel, with respect to the luminosity center, and I_k its intensity. The luminosity center is defined as

$$\begin{aligned} x_{lc} &= \frac{\sum_{i=0}^{500} \sum_{j=0}^{500} f(x,y) I_{xy} x}{\sum_{i=0}^{500} \sum_{j=0}^{500} f(x,y) I_{xy}} \\ y_{lc} &= \frac{\sum_{i=0}^{500} \sum_{j=0}^{500} f(x,y) I_{xy} y}{\sum_{i=0}^{500} \sum_{j=0}^{500} f(x,y) I_{xy}} \end{aligned}$$

with I_{xy} equal to the pixel intensity value and $f(x,y)$ equal to 0 or 1 depending if the pixel is inside or outside of the ROI, respectively.

G. Entropy of the Contour Gradient

In Fig. 7, a pixel of the contour is shown by the black square. The related gradient value will be oriented in the direction of the maximum change, among the eight neighbors.

The entropy E_C for the direction of the gradient contour is obtained by building the histogram of the gradient direction for all the contour pixels for a ROI

$$E_C = - \sum_{k=1}^8 p_k \log(p_k)$$

where p_k is the probability that the gradient direction will be oriented in the direction k , with $k = 1, \dots, 8$. The E_C entropy measure carries information on the roughness of the ROI contour.

H. Anisotropy

Another parameter which may give information about the irregularity of the ROI is the distance between the geometric

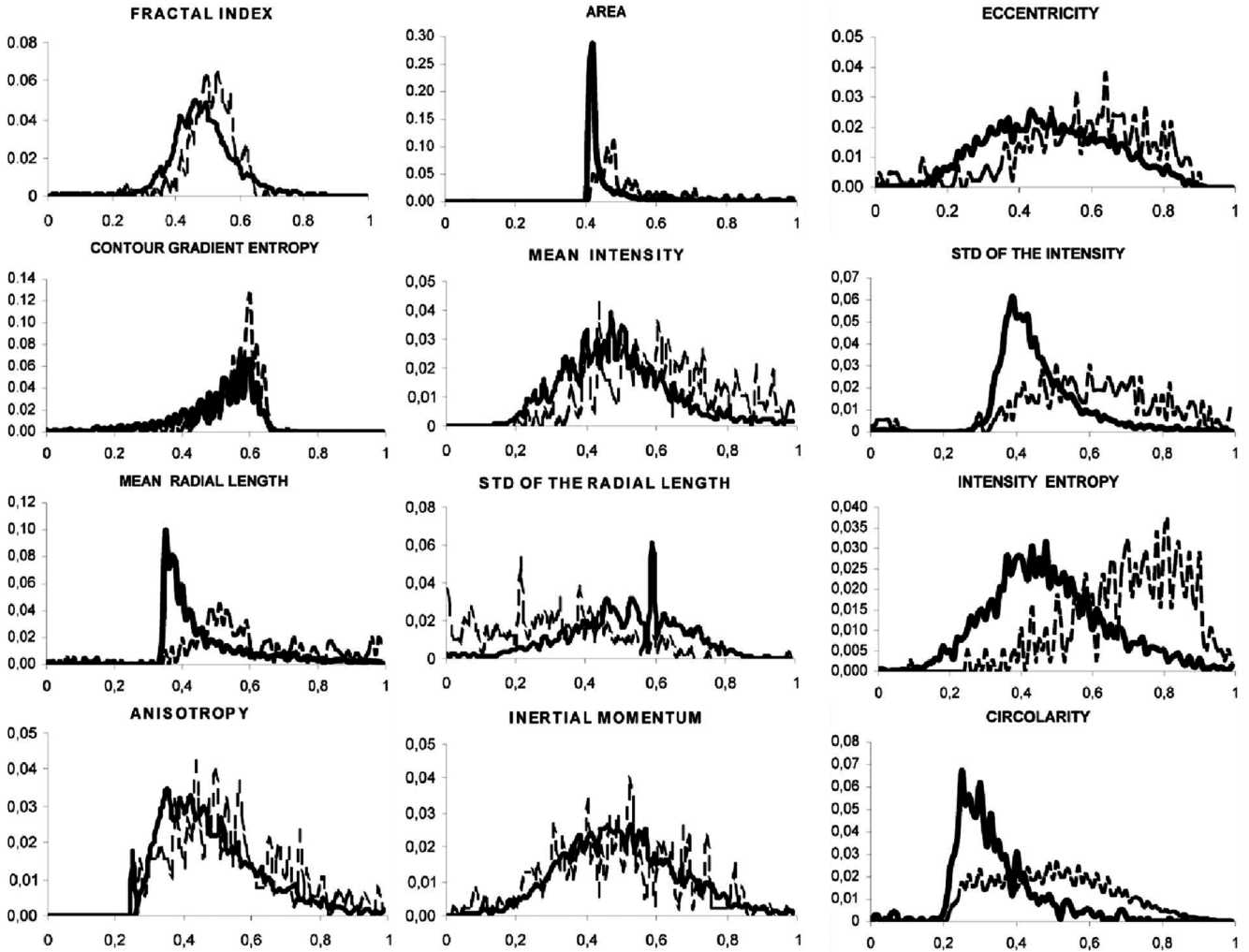


Fig. 8. Histograms normalized, for pathological (dashed line) and healthy (continuous bold line) ROIs.

center and the center of luminosity. If the shape of a ROI have an isotropic symmetry this distance is close to zero while it increases at higher distortion.

I. Mean and Standard Deviation of the Intensity

The mean and the standard deviation of the pixels intensity are given by

$$I = \frac{1}{M} \sum_{k=1}^M I_k \quad \sigma = \sqrt{\frac{1}{M} \sum_{k=1}^M (I_k - I)^2}$$

where I_k is the value of the intensity of the k_{th} pixel and M is the number of the pixels of the ROI.

J. Area

The ROI area is defined as the total number of the pixels delimited by the ROI contour. This value is suitably normalized.

Features Performance Evaluation

The variability range varies from feature to feature and the healthy/pathological data histograms show a different shape, as showed in Fig. 8. Moreover, the number of healthy ROI is about

seven times bigger than the number of pathological ROI. For this reason each feature histogram is normalized both to its minimum and maximum values, and to the total ROI number in each class.

A completely overlapped histogram for the healthy/pathological classes, corresponds to a feature not being able to discriminate the presence of a pathology, while a reduced value of the overlapping area indicates an increased discrimination capability.

Each feature discrimination value was evaluated by using a KNN classifier and by calculating the twelve ROC corresponding curves.

For a feature with randomly distributed discrimination capability, the ROC curve area A_z ranges around 50%. For this reason we decided to split all features in three classes: low separability ($A_z < 65\%$), standard separability ($65\% < A_z < 75\%$), high separability ($A_z > 75\%$). With these criteria we get

- low separability (area, inertial momentum, entropy of contour gradient, anisotropy)
- normal separability (fractal index, eccentricity, mean intensity, std of the radial length)
- high separability (std of the intensity, mean radial length, entropy of intensity distribution, circularity).

TABLE II
INPUT DATASET TO THE NEURAL NETWORK

	<i>Dataset</i>	<i>Pathological sample</i>	<i>Healthy sample</i>
<i>Training set</i>	I	454	1961
<i>Validation set</i>	I	114	476
<i>Test set</i>	II	583	7940

Even if every feature of the first group has low discrimination capability by itself, all the four contribute in meaningful way to the final ROC curve; this is the reason for which it was decided to keep using them.

V. CLASSIFICATION

As aforementioned, all the pathological database mammographies have been marked by a doctor by drawing a circle of radius ROI_{Rad} around existing lesions; in order to get a better estimation for the lesion center, we retrieve within this circle the luminosity center.

All the ROIs extracted from healthy patient images are tagged as negatives (FP), while the ROIs selected by the CAD from the pathological image are to be labeled as true positive (TP) if they meet at least one of the following criteria:

- the ROI_{Rad} center lies inside the ROI_{CAD} ;
- the ROI_{CAD} center lies inside the ROI_{Rad} .

In both cases, the radius ratio

$$r = \frac{\min [R_{Rad}, R_{CAD}]}{\max [R_{Rad}, R_{CAD}]}$$

must be higher than 0.5 to get a more restrictive condition. We did not use in training phase those ROIs which overlapped with radiologist circles but were not satisfying the aforementioned significance condition.

The classification is performed by means of an Artificial Neural Network [18]–[20] with 12 input neurons, a number of hidden neurons which is tuned to obtain the best classification performance, and 1 output neuron.

The neural network gradually modifies the weights of the connections through a repeated presentation of a set of input patterns (learning set), with a prescribed answer, which is 1 for pathological patterns, 0 otherwise. This process is known as supervised learning. The weight modification is achieved through minimization of the difference between the neural output and the answer prescribed by the “teacher.”

In our case, the dataset is made of 1151 pathological and 10 377 healthy patterns, extracted from images related to 1093 subjects. Within the dataset, pathological patterns correspond to the radiologist’s positive diagnosis, while healthy ones come from images without any lesion at all. The aforementioned dataset was randomly split in learning and test subsets. The pathological and healthy samples were extracted as reported in Table II.

The neural output provides a continuous value $0 < P < 1$ which is used as a threshold to discriminate between mass regions and healthy ones. For each threshold value, the sensitivity and the specificity are computed.

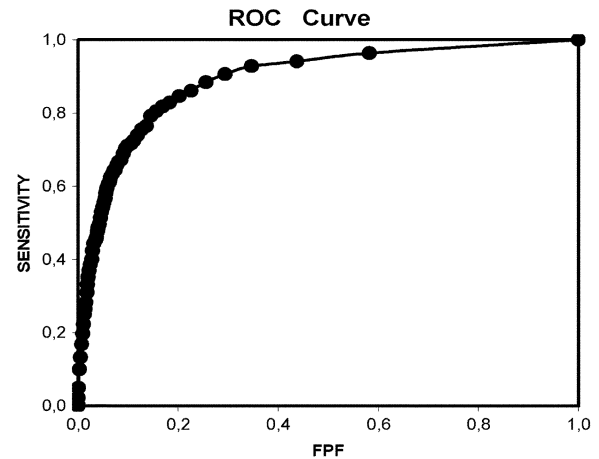


Fig. 9. ROC Curve.

The adopted Neural Network is a feedforward backpropagation supervised network trained with gradient descent learning rule with “momentum,” to quickly move along the direction of decreasing gradient, thus, avoiding oscillations around secondary minima. The software is SNNS v4.1 (Stuttgart University). The weights were determined by training the network with the *training set* and minimizing the mean squared error (MSE) of the *validation set*. The minimum MSE value was achieved after 500 learning epochs.

VI. RESULT AND DISCUSSION

The classification was performed on the *test set* in Table II, and the results obtained with this system are reported in Fig. 9 in terms of the ROC curve. The performance is quantified by the value of the area A_z [21], [22] under the curve

$$A_z = 0.862 \pm 0.007.$$

This value is an index of the discrimination capability between true masses and false-positive detection. This result refers to the neural network classification only.

The performance of the whole CAD system, including the ROI Hunter efficiency, is reported in Fig. 10 in terms of the FROC curve, where the maximum sensitivity value is compatible with the ROI Hunter efficiency ($\varepsilon = 93\%$). As it is visible in Fig. 10, we get a 2.8 FP/Image at a sensitivity of 82%. The capability to set a threshold value on the Neural Network output allows us to chose the best CAD working point in order to tune the performance versus the radiologist’s request (screening, clinic application, etc.).

These results showed that the features chosen are able to distinguish pathological lesions from the healthy ones. In future studies, additional information will be included to improve differentiation among different kinds of tumors.

Moreover, feature selection process using an algorithm such as linear discriminating analysis can provide additional means to aid the radiologist in diagnosing breast disease.

The positive results obtained with the features based on tumor shape is a promising starting point for the future perspectives.

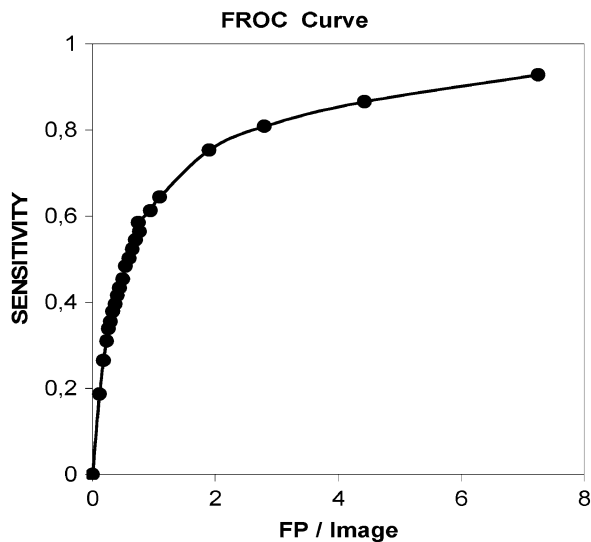


Fig. 10. FROC Curve.

VII. CONCLUSION

In this paper an algorithm for mass lesions detection has been presented. This algorithm relies on an edge-based threshold operator strategy for the mass segmentation. From the selected ROIs 12 features are extracted to discriminate between the two classes (pathological patients or healthy subjects). The discriminating performance of the algorithm has been checked by means of a supervised Neural Network and the results have been presented in terms of ROC and FROC curves. The value of the area A_z under ROC curve is comparable with the performance obtained by commercial CAD [23].

The algorithm has been designed in the framework of the INFN MAGIC-5 project (Medical Applications on a Grid Infrastructure Connection), which aims at developing a CAD system for early diagnosis of breast cancer. A CAD Station running this software is actually working in the hospitals belonging to the MAGIC-5 collaboration and has been positively evaluated by medical users.

ACKNOWLEDGMENT

The authors are grateful to the staff and the institutions involved in the study for their precious help and support. In particular, they thank Prof. V. Lattanzio (Policlinico di Bari), Prof. Bazzocchi (Dipartimento di Ricerche Mediche e Morfologiche della Università, Udine, Italy), Prof. E. Zanon (Ospedale Valdese di Torino and INFN, sezione di Torino), Prof. A. Sodano (Dipartimento di Scienze Biomorfologiche e Funzionali Università di Napoli "Federico II" Napoli, Italia) and Prof. R. Lagalla, Dr. R. Ienzi, Dr. G. Bellissima, Dr. V. Ricotta (Istituto di Radiologia P. Cignolini—University of Palermo) for the medical support in the data acquisition.

REFERENCES

- [1] F. Levi, F. Lucchini, E. Negri, P. Boyle, and C. La Vecchia, "Mortality from major cancer sites in the European Union, 1955–1998," *Ann. Oncol.*, vol. 14, pp. 490–495, 2003.
- [2] L. W. Bassett, R. H. Gold, and C. S. Kimme, "History of the technical development of mammography," *Syllabus: A Categorical Course in Physics RSNA*, 1994.
- [3] L. Tabar, C. J. G. Fageberg, and A. Grad, "Reduction in mortality from breast cancer after mass screening with mammography randomised trial from the breast cancer screening working group of the Swedish national board of health and welfare," *Lancet*, vol. 829, p. 8433, 1985.
- [4] R. Bird, T. Wallace, and B. Yankaskas, "Analysis of cancer missed at screening mammography," *Radiology*, vol. 184, pp. 613–617, 1992.
- [5] S. Timp and N. Karssemeijer, "A new 2D segmentation method based on dynamic programming applied to computer aided detection in mammography," *Med. Phys.*, vol. 31, pp. 958–971, 2004.
- [6] A. H. Baydush, D. M. Catarious, C. K. Abbey, and C. E. Floyd, "Computer aided detection of masses in mammography using subregion Hotelling observers," *Med. Phys.*, vol. 30, pp. 1781–1787, 2003.
- [7] G. D. Tourassi, R. Vargas-Voracek, D. M. Catarious, Jr., and C. E. Floyd, Jr., "Computer-assisted detection of mammographic masses: A template matching scheme based on mutual information," *Med. Phys.*, vol. 30, no. 8, pp. 2123–2130, 2003.
- [8] J. K. Kim and H. W. Park, "Statistical textural features for detection of microcalcification in digitized mammograms," *IEEE Trans. Med. Imag.*, vol. 18, no. 3, Mar. 1999.
- [9] N. Karssemeijer, "Automated classification of parenchymal pattern in mammograms," *Phys. Med. Biol.*, vol. 43, p. 365, 1998.
- [10] M. Bazzocchi, I. Facecchia, C. Zuiani, V. Londero, S. Smania, U. Bottigli, and P. Delogu, "Application of a computer-aided detection (CAD) system to digitalized mammograms for identifying microcalcifications," *Radiol. Med.*, vol. 101, pp. 334–340, 2001.
- [11] M. E. Fantacci, U. Bottigli, P. Delogu, F. Fauci, B. Golosio, A. Lauria, R. Palmiero, G. Raso, S. Stumbo, and S. Tangaro, "Search of microcalcifications clusters with the CALMA CAD station," *Proc. SPIE*, vol. 4684, pp. 1301–1310, 2002.
- [12] S. R. Amendolia, U. Bottigli, A. Ceccopieri, P. Delogu, G. Dipasquale, M. E. Fantacci, A. Marchi, V. M. Marzulli, P. Oliva, V. Rosso, A. Stefanini, and S. Stumbo, "Comparison of imaging properties of several digital radiographic system," *Nucl. Instrum. Methods Phys. Res. A*, vol. 466, pp. 95–98, 2001.
- [13] N. Wolfe, "Risk for breast cancer development determined by mammographic parenchymal pattern," *Cancer*, vol. 37, pp. 2486–2492, 1976.
- [14] C. Frouge, *Strategia Diagnostica in Senologia*, Masson, Milano-Pari—Barcelona, 1998.
- [15] M. L. Antonie, O. R. Zaiane, and A. Coman, "Application of data mining techniques for medical image classification," in *Proc. II Int. Work. On Multimedia Data Mining*, 2001.
- [16] C. J. Vyborny and M. L. Giger, "Computer vision and artificial intelligence in mammography," *AJR*, vol. 162, pp. 699–708, 1994.
- [17] S. Lai, X. Li, and W. Bischof, "On techniques for detecting circumscribed masses in mammograms," *IEEE Trans. Med. Imag.*, vol. 8, no. 4, pp. 377–386, 1989.
- [18] D. S. Haykin, *Neural Networks: A Comprehensive Foundation*. New York: McMillan, 1994.
- [19] D. Floreno, 1996, *Manuale sulle reti neurali*, Il Mulino.
- [20] A. Zell, G. Mamier, M. Vogt, N. Mache, R. Hubner, S. Doring, K. U. Herrmann, T. Soye, M. Schmalzl, T. Sommer, A. Hatzigeorgion, D. Posselt, T. Schreiner, B. Kett, G. Clemente, and J. Wieland SNNS, *Stuttgart Neural Network Simulator*. Stuttgart: Univ. Stuttgart, 1995, User Manual, Version 4.1.
- [21] J. A. Hanley and B. McNeil, "The meaning and use of the area under a receiver operating characteristic (ROC) curve," *Radiology*, vol. 143, pp. 29–36, 1982.
- [22] J. A. Hanley and B. McNeil, "A method of comparing the areas under receiver operating characteristic curves derived from the same cases," *Radiology*, vol. 148, pp. 839–843, 1983.
- [23] A. Malich, C. Marx, and M. Facius, "Tumour detection rate of a new commercially available computer-aided detection system," *Eur. Radiology*, vol. 11, no. 12, pp. 2454–2459, 2001.